The Journal of Chemical Physics

Theoretical studies of the vibrational properties of octahedrane ($C_{12}H_{12}$): A polyhedral caged hydrocarbon molecule

Cite as: J. Chem. Phys. **150**, 214304 (2019); https://doi.org/10.1063/1.5096404
Submitted: 17 March 2019 . Accepted: 11 May 2019 . Published Online: 05 June 2019

Daniel Finkenstadt, Michael J. Mehl, Mark R. Pederson, and Steven L. Richardson

The Journal of Chemical Physics ARTICLE scitation.org/journal/jcp

Theoretical studies of the vibrational properties of octahedrane ($C_{12}H_{12}$): A polyhedral caged hydrocarbon molecule

Cite as: J. Chem. Phys. 150, 214304 (2019); doi: 10.1063/1.5096404
Submitted: 17 March 2019 • Accepted: 11 May 2019 •
Published Online: 5 June 2019

Daniel Finkenstadt,[1,2] Michael J. Mehl,[1,2] Mark R. Pederson,[3] and Steven L. Richardson[2,4,5,a)]

AFFILIATIONS

[1]U.S. Naval Academy, Department of Physics, Annapolis, Maryland 21402, USA
[2]U.S. Naval Research Laboratory, Center for Computational Materials Science, Washington, DC 20375, USA
[3]U.S. Department of Energy, Office of Basic Energy Sciences, Washington, DC 20585, USA
[4]Department of Electrical and Computer Engineering, Howard University, 2300 Sixth Street NW, Washington, DC 20059, USA
[5]Department of Chemistry, Massachusetts Institute of Technology, Cambridge, Massachusetts 02139, USA

[a)]**Author to whom correspondence should be addressed:** srichards22@comcast.net. **Fax:** 1 301 879-2029.

ABSTRACT

The vibrational properties of octahedrane ($C_{12}H_{12}$) are calculated using density-functional theory employing two different computational methods: an all-electron Gaussian orbital approach and a Naval Research Laboratory-tight-binding scheme (NRL-TB) coupled with molecular dynamics (NRL-TBMD). Both approaches yield vibrational densities of states for octahedrane that are in good general agreement with each other. NRL Molecular Orbital Library can also provide accurate infrared and Raman spectra which can be analyzed and compared with experimental results, while NRL-TBMD can be conveniently scaled up for larger finite-temperature simulations. This latter approach is used in our paper to produce a theoretical prediction for a stable room temperature structure of octahedrane.

https://doi.org/10.1063/1.5096404

I. INTRODUCTION

Polyhedral caged hydrocarbon molecules are quite interesting to explore because of their unique shapes and symmetries. One such molecule is octahedrane ($C_{12}H_{12}$, D_{3d}) [cf. Figs. 1 and 2(a)] which contains two three-membered cyclopropyl rings that are connected by six fused five-membered cyclopentyl rings. A six-membered cyclohexyl ring in the chair conformation is located at the equatorial region of the molecule.

Octahedrane was first synthesized by Lee *et al.* in 1993,[1] although an important skeleton of octahedrane, 2,9-dimethyl-*p*-[$3^2{\cdot}5^6$] octahedrane, was first synthesized by Hirao *et al.*[2] a year earlier. Remarkably, both of these multistep synthetic approaches have been surpassed with an amazing one-step photochemical reaction by Okamoto *et al.* in 2006[3] to produce the octahedrane framework. Although octahedrane is a highly strained polyhedral hydrocarbon caged molecule, it is interestingly enough quite a kinetically stable solid at room temperature with a decomposition temperature at or above 180 °C. While octahedrane is not believed to be a naturally occurring molecule, it may have important applications in many areas including nanoscale energy storage and fuel combustion enhancement. Furthermore, the unique shape and caged structure of octahedrane could be useful in biomedical applications.

The theoretical work by de Meijere *et al.*[4] using density-functional theory (DFT)[5,6] has shown that octahedrane is more strained than the structurally related molecule decahedrane ($C_{16}H_{16}$, D_{4d}) [cf. Fig. 2(b)], which has two four-membered cyclobutyl rings which are connected by eight fused five-membered cyclopentyl rings, and the famous Platonic solid dodecahedrane ($C_{20}H_{20}$, I_h) [cf. Fig. 2(c)]. Dodecahedrane was first synthesized by Paquette *et al.* in 1982[7] and contains 12 fused five-membered cyclopentyl rings. de Meijere and his collaborators[4] have also successfully functionalized octahedrane through bromination and studied the stability of a variety of brominated adducts using DFT. More recent studies[8] have examined the heats of formation of platonic hydrocarbons, including octahedrane.

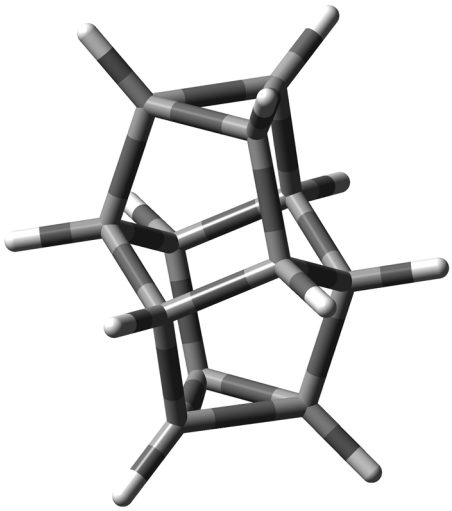

FIG. 1. Structure of octahedrane ($C_{12}H_{12}$).

We have previously used DFT and a general *ab initio* parameterized tight-binding model for hydrocarbons[9,10] to calculate the structural, electronic, and vibrational properties of a number of important hydrocarbons including cubane,[10,11] its related high-energy density material octanitrocubane,[12] adamantane,[13] and cyclohexamantane.[13,14] Furthermore, we have used a very large basis set of Gaussian orbitals for our atoms at a level of theory using the Perdew-Burke-Ernzerhof generalized-gradient approximation (PBE-GGA) for the exchange and correlation functional[15,16] in our calculations to compute vibrational properties, such as the infrared and Raman spectra, which are in very good agreement with the experiment. This is interesting despite the results of some previous studies[17,18] which have questioned the reliability of using some common GGAs and hybrid functionals to predict the total energy differences among hydrocarbon isomers.

Since there are no published experimental or theoretical vibrational spectra for octahedrane, we believe this study provides another excellent opportunity to provide accurate vibrational spectra for future experimental and theoretical work on other hydrocarbons with unique shapes and symmetries. In our computational study, we chose two different methods to calculate the structural, electronic, and vibrational properties of octahedrane.

We employed an all-electron DFT approach using the Naval Research Laboratory Molecular Orbital Library (NRLMOL) suite of programs,[19–21] which has the advantage of yielding accurate infrared and Raman frequencies and intensities for molecules and clusters. In addition, we used the NRL tight-binding scheme (NRL-TB)[22–27] which is parameterized from a number of previous all-electron DFT studies of a small library of simpler molecules and crystalline structures. The tight-binding method can produce structural and electronic information for octahedrane computationally faster than NRLMOL, although it yields a vibrational density of states (VDOS) which cannot be easily decomposed into infrared and Raman active modes. On the other hand, the tight-binding parameters work well for large periodic solid structures, which is the focus of future discussions on the solid state properties of octahedrane. Both schemes give VDOS that are comparable with each other and provide important results for further experiments.

II. METHODOLOGY

A. The NRLMOL approach

The first-principles DFT calculations were performed with the all-electron Naval Research Laboratory Molecular Orbital Library (NRLMOL) suite of programs.[19–21] This present study used PBE-GGA for the exchange and correlation density-functional,[15,16] and a massively parallelized version of NRLMOL was used throughout this work.[28] The Kohn-Sham orbitals were expressed as a linear combination of atomic orbitals, where an orbital is expanded in a Gaussian basis set centered about each atom. This basis set has been successfully applied to other hydrocarbons using NRLMOL,[13,14] as well as

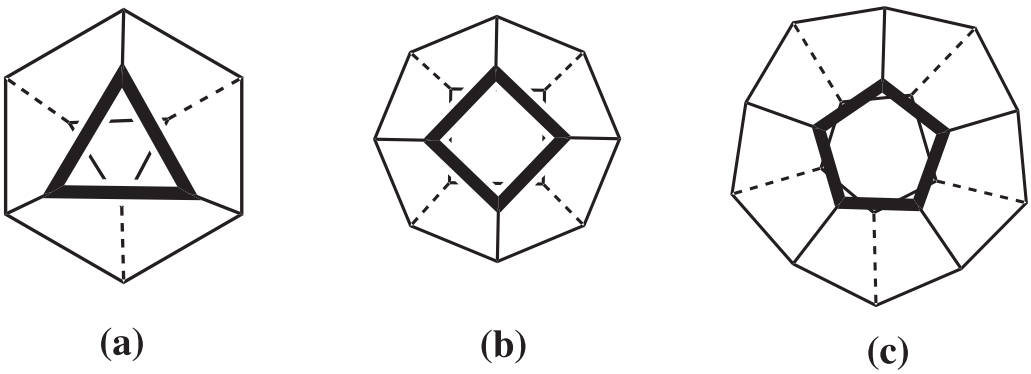

FIG. 2. Illustrations of the polyhedral caged hydrocarbons octahedrane, decahedrane, and dodecahedrane when viewed along the C_n (n = 3, 4, and 5, respectively) molecular axis which passes through the top and bottom rings of the molecules. The hydrogen atoms are not shown for the sake of clarity. (a) $C_{12}H_{12}$. (b) $C_{16}H_{16}$. (c) $C_{20}H_{20}$.

to other high-energy density molecules.[29–33] The multicenter integrals required to solve the Kohn-Sham equation were calculated by numerically integrating over a mesh of points.[19]

Octahedrane was optimized using the Hellmann-Feynman-Pulay forces[34,35] in conjunction with the limited-memory Broyden-Fletcher-Goldfarb-Shanno (LBFGS) scheme of minimization. A final, optimized geometry was obtained when the total forces were less than 0.001 hartree/bohr. For each geometry, the SCF cycle was carried out until the energy differences were less than 10^{-6} hartree.

The vibrational frequencies were calculated by direct diagonalization of the dynamical matrix. This matrix is constructed by taking finite differences of both positive and negative displacements (ranging from 0.02 to 0.05 a.u.) of the coordinates of each atom near the equilibrium geometry and calculating the forces for each corresponding geometry. The optimized structure for octahedrane was found to be vibrationally stable with no imaginary frequencies. The infrared and Raman intensities discussed here were obtained from derivatives with respect to the atomic coordinates of the dipole moment and the polarizability tensor. A more detailed description of the methods used here is provided in Refs. 36–38.

B. The NRL-TB and NRL-TBMD methods

An alternative approach to determine the electronic structure of octahedrane is the NRL tight-binding (NRL-TB) scheme.[22–27] The primary advantage of the NRL-TB method is that, coupled with the tight-binding molecular dynamics code (NRL-TBMD),[39,40] one can rapidly determine the static and dynamic properties of a particular molecule or material much faster than DFT schemes, like NRLMOL, at finite temperatures. The NRL-TB method has been shown to yield accurate electronic structure and total energies for transition metals,[41] semiconductors, bulk graphite,[42] C_{60}, and nanotubes.

To produce electronic structure results that are of the same level of accuracy as DFT, we fit the C–C tight-binding parameters in NRL-TB to a set of linearized augmented plane-wave results[43,44] for over a wide range of volumes for diamond, graphite, and simple cubic crystal structures, and for a range of interatomic distances within the C_2 molecule, as computed with NRLMOL. Within the NRL-TB method, we modeled the carbon atoms using one *s* and three *p* orbitals and the hydrogen atom with one *s* orbital.

The H–H tight-binding parameters were fit to molecular orbital energy levels for H_2 and a H_6 ring. The NRL-TB method allows some latitude in the choice of the zeros of the total energy for the individual atomic species.[22,23] We adjusted the energy of H_2 so that the energy difference between the bonding orbital of the H_2 molecule and the lowest 2*s* orbital of C_2 was the same as in NRLMOL. This assured that no artificial charge transfer occurs from C to H_2 at large separations. We determined the C–H tight-binding parameters by freezing the C–C and H–H parameters and subsequently fitting the remaining parameters to NRLMOL results for the molecules: methane, ethane, ethylene, and benzene.

The tight-binding parameters for the C–C, H–H, and C–H interactions have been previously shown to reproduce the correct equilibrium structures for graphene sheets, ribbons, and flakes,[9] as well as for many other hydrocarbons.[10] Given the very transferable set of NRL-TB tight-binding parameters for hydrocarbons, we then applied them to the polyhedral caged hydrocarbon, octahedrane, and found an optimized geometry for the molecule.

1. Timing considerations

To give a rough quantitative estimate of how much the computations are sped up by using the NRL-TBMD scheme, we typically have to diagonalize a $(5N) \times (5N)$ matrix, where N is the number of C–H dimers in the system. This time scales as the size of the matrix cubed, in this case $125N^3$. For commercial DFT software, you might also diagonalize a large (say) 1000×1000 matrix, at a time cost of 10^9, but the increase in matrix size with the number of dimers might be large. To give real numbers, our TBMD calculations required roughly 5 s/iteration for 648 ions, or 1620 electrons, on 32 processors. An identical system calculated using DFT on 32 processors might take up to 24 h/iteration, depending on the software. Moreover, the memory and cache limitations might become problems even before time does.

2. NRL-TBMD simulation of octahedrane

For the NRL-TBMD simulation of octahedrane, a large supercell was constructed containing 27 octahedrane molecules, or 648 atoms, in a very low-density cubic arrangement to nullify the interaction between molecules. We used the same starting geometry for octahedrane in the MD simulation as we did for the NRLMOL calculation. This supercell constitutes a thermodynamic ensemble for the purposes of calculating random vibrational excitations of molecules at finite temperature, which in this computational study is at 300 K. To minimize the computational cost of long MD runs, *only* the Γ-point was used for the Brillouin zone *k*-point integration during the MD simulations. Random velocities were chosen to achieve the desired equilibrium temperature. In all systems, the MD runs were for 20 000 time steps of $\Delta t = 0.5$ fs, giving a total simulation time of 10 ps. The equations of motion were integrated using the Verlet algorithm. The first 2000 time steps were discarded for thermal equilibration, and the remaining steps were kept and used for the analysis of the dynamical properties of octahedrane.

To analyze the VDOS, we used the velocity-autocorrelation (VAC) method, as derived in Ref. 45, and applied more recently using NRL-TBMD to transition metals.[41] The VAC method is essentially a time-domain Fourier transform of the velocity-related quantities from MD, namely,

$$\mathrm{VDOS}\ (\omega) \propto \int_0^\infty \mathrm{d}t\, e^{-i\omega t} \sum_{i=1}^{N} \langle \mathbf{v}_i(t) \cdot \mathbf{v}_i(0) \rangle,$$

where $\mathbf{v}_i(t)$ are the ionic velocities of the N ions, and the average is taken over the total simulation time T, namely,

$$\langle \mathbf{v}(t) \cdot \mathbf{v}(0) \rangle = \frac{1}{T} \int_{-T}^{T} \mathrm{d}t'\, \mathbf{v}(t+t') \cdot \mathbf{v}(t').$$

This method produces a similar dispersion and a VDOS as other methods, such as the frozen-phonon approach, but it has the advantage of identifying vibrational properties in larger cells that are difficult to capture using other methods.[10]

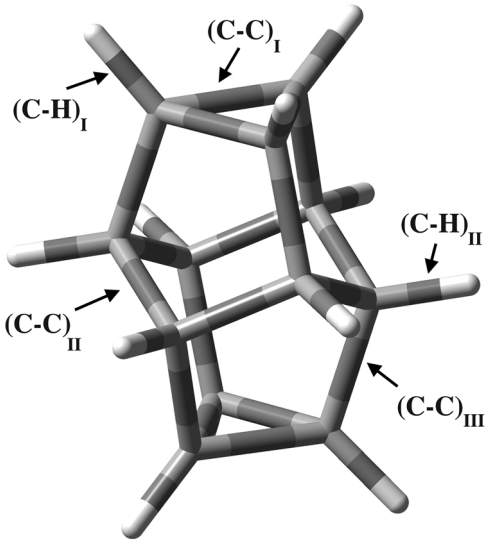

FIG. 3. Structure of octahedrane ($C_{12}H_{12}$).

III. GEOMETRY OPTIMIZATION

Octahedrane contains two distinct types of chemical bonds: C–H and C–C bonds. Each of these two bonds can be further classified as follows. We define the $(C–H)_I$ and $(C–C)_I$ bonds as those which lie within each of the two cyclopropyl rings that are intersected by the C_3 molecular axis, as shown in Figs. 2(a) and 3. We also illustrate in Fig. 3 an equatorial cyclohexyl ring that contains two different types of bonds which we will define as $(C–H)_{II}$ and $(C–C)_{II}$. Finally, octahedrane has six C–C bonds which connect the two cyclopropyl rings to the equatorial cyclohexyl ring. We will define those types of bonds as $(C–C)_{III}$. The results of using both NRLMOL and NRL-TBMD to optimize octahedrane are shown in Table I and are in excellent agreement with available solid state x-ray diffraction data for the molecule. In Table II, we show the computed binding energy and HOMO-LUMO gap using NRLMOL for molecular octahedrane and NRL-TBMD for both the molecular and solid state phases of octahedrane. The NRLMOL calculations yielded a very small dipole moment for octahedrane of magnitude 0.001 87 D and a polarizability tensor whose components are α_{xx} = 18.571 36, α_{xy} = 0.012 577, α_{xz} = 0.011 597, α_{yx} = 0.012 577, α_{yy} = 16.653 67, α_{yz} = 0.010 929, α_{zx} = 0.011 597, α_{zy} = 0.010 929, and α_{zz} = 16.641 49. The NRLMOL calculated electron affinity for octahedrane (+1.047 eV) is positive, as expected.

TABLE I. Calculated bond lengths of octahedrane, corresponding to Fig. 3 (units of Å).

Bond classification	Bond length (NRLMOL)	Bond length (NRL-TBMD)	Experimental (Ref. 4)
$(C–H)_I$	1.09	1.10	n.r.
$(C–H)_{II}$	1.10	1.11	n.r.
$(C–C)_I$	1.52	1.47	1.51
$(C–C)_{II}$	1.56	1.55	1.55
$(C–C)_{III}$	1.53	1.52	1.52

TABLE II. Calculated electronic structure of octahedrane in units of eV per molecule (solid state results in parentheses).

	NRLMOL	NRL-TBMD
Binding energy	−122.282	−164.64 (−166.065 as solid)
HOMO-LUMO gap	5.67	6.40 (5.27 as solid)

For the crystalline structure, a set of candidate unit cells were constructed and relaxed to reduce forces to less than 10^{-2} eV/Å and stresses to less than 10^{-3} eV/Å^3. Beginning with a 2 × 2 × 2 supercell containing 192 atoms, the lowest energy structure was triclinic with the $P\bar{1}$ space group, as shown in Fig. 4. This cell contains 24 atoms and only has inversion symmetry from a point within the center of the cell. In Fig. 5, we have provided a more detailed picture for this triclinic unit cell with the hydrogen atoms omitted for the sake of clarity. In our simulations, the hydrogen atoms appear in different locations than in the molecule due to periodic boundary conditions and orthographic projection, but they are, in fact, coordinated nearly identically to the free molecule. A density of 1.7 g/cm^3 was found at equilibrium. This density, at which the solid starts to form, is approximately 1 molecule per 125 Å^3, which is a large volume (5 Å)^3, considering that the largest distance between atoms across the molecule is roughly 6 Å. These estimated quantities should not be taken too literally since the LDA is known to overestimate densities in many systems, and van der Waals interactions in solids are a challenge to estimate from first principles. More detailed studies of solid octahedrane will be detailed in a separate publication. The calculated solid structure may be stable as it has no zone-centered imaginary phonons; however, it does have some off-diagonal elastic

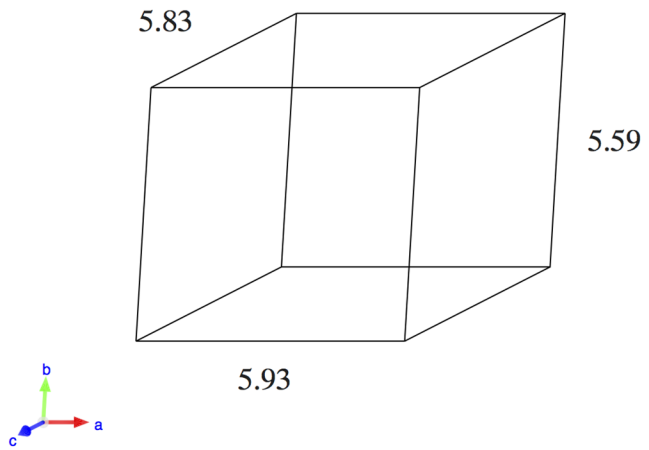

FIG. 4. Optimized triclinic unit cell of solid octahedrane with geometric lattice parameters indicated. Cell angles are α = 108.2°, β = 123.4°, and γ = 86.6°. Cell size is in Å.

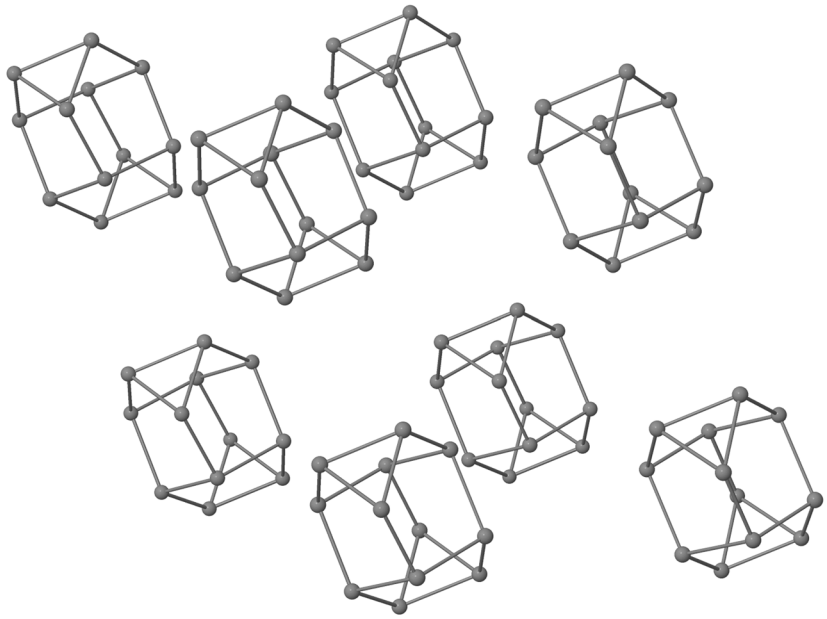

FIG. 5. Illustration of the 2 × 2 × 2 supercell of solid octahedrane with a selection of eight octahedrane molecules at the corners of a triclinic unit cell. The hydrogen atoms are omitted for the sake of clarity.

constants approaching zero within the accuracy of the calculation, making solid octahedrane likely a soft material with respect to some shear moduli. The details of the elastic and phonon structure will be pursued in a later publication.

Although there is no solid state data available, a comparison with Ref. 46 confirms that a dimer of octahedrane molecules is bound with weak but nonvanishing dihydrogen intermolecular bonding. We find a similar close-spacing dimer structure for neighboring octahedrane molecules along the same intermolecular direction as in our solid state calculation.

IV. VIBRATIONAL ANALYSIS

The calculated infrared and Raman spectra for octahedrane using NRLMOL are shown in Fig. 6. At this time, there are no published experimental data to compare our theoretical predictions with. Both of these vibrational spectra show a common set of features: low frequency modes from 560 cm^{-1} to 1355 cm^{-1} due primarily to strong C–C stretches and significant distortions of the core carbon framework of octahedrane; a desert region between 1355 cm^{-1} and 3006 cm^{-1}; and a set of high frequency modes

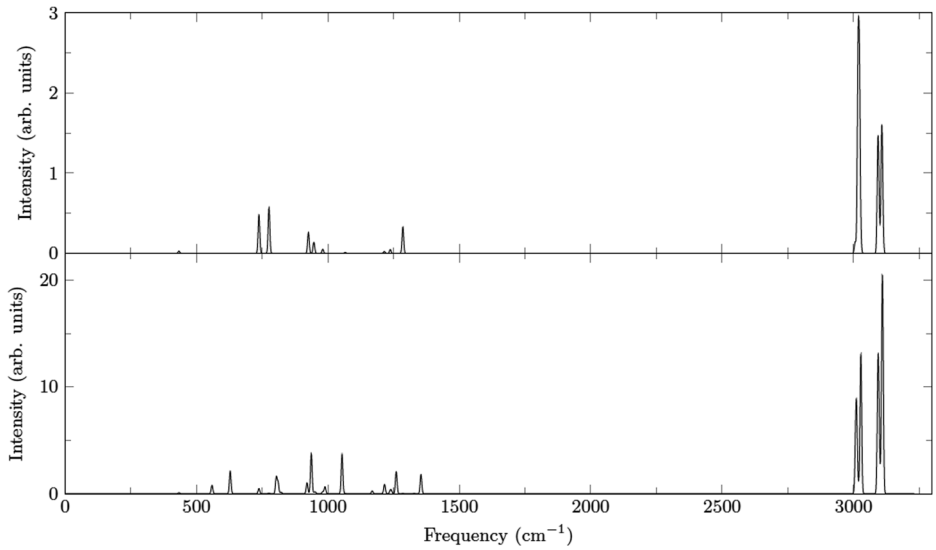

FIG. 6. Calculated DFT IR and Raman spectra for octahedrane ($C_{12}H_{12}$). A Gaussian broadening of 6 cm^{-1} was used for both spectra.

TABLE III. Listing of theoretical infrared (IR) and Raman frequencies and intensities for octahedrane ($C_{12}H_{12}$). All infrared and Raman frequencies are reported in units of cm^{-1}. Qualitative physical descriptions for our theoretical infrared and Raman modes were obtained using the software package iMol.[47] vs = very strong, s = strong, m = medium, w = weak, and sh = shoulder peak.

Theoretical IR	Theoretical Raman	Mode description
	560 (w)	Breathing mode with a large distortion of the C–C–C framework, Weak asynchronous $(C–H)_I$ and $(C–H)_{II}$ stretches With weak $(C–H)_I$ and medium $(C–H)_{II}$ wagging, Strong $(C–C)_I$, medium $(C–C)_{II}$, and weak $(C–C)_{III}$ stretches
	629 (m)	Breathing mode along the axis through cyclopropyl and cyclohexyl rings, Weak asynchronous $(C–H)_I$ and $(C–H)_{II}$ stretches With medium $(C–H)_I$ and strong $(C–H)_{II}$ wagging, Strong $(C–C)_{II}$ and $(C–C)_{III}$ stretches
738 (m)	738 (w)	Weak asynchronous $(C–H)_I$ stretches with strong $(C–H)_I$ and medium $(C–H)_{II}$ wagging, Weak $(C–C)_I$, $(C–C)_{II}$ stretches, and $(C–C)_{III}$ stretches
776 (m)		Weak asynchronous $(C–H)_I$ stretches with weak $(C–H)_I$ and $(C–H)_{II}$ wagging, Strong $(C–C)_I$ and weak $(C–C)_{II}$ and $(C–C)_{III}$ stretches
	808 (m)	Weak asynchronous $(C–H)_I$ and $(C–H)_{II}$ stretches With medium $(C–H)_I$ and strong $(C–H)_{II}$ wagging, Weak $(C–C)_I$, strong $(C–C)_{II}$, and weak $(C–C)_{III}$ stretches
	921 (w)	Weak asynchronous $(C–H)_I$ and $(C–H)_{II}$ stretches With strong $(C–H)_I$ and medium $(C–H)_{II}$ wagging, Weak $(C–C)_I$, medium $(C–C)_{II}$, and strong $(C–C)_{III}$ stretches
926 (w)		Breathing mode along the axis through cyclopropyl and cyclohexyl rings, Weak asynchronous $(C–H)_I$ and $(C–H)_{II}$ stretches With weak $(C–H)_I$ and strong $(C–H)_{II}$ wagging, Strong $(C–C)_I$ and $(C–C)_{III}$ stretches
	937 (m)	Weak asynchronous $(C–H)_I$ and $(C–H)_{II}$ stretches With medium $(C–H)_I$ and strong $(C–H)_{II}$ wagging, Strong $(C–C)_I$, weak $(C–C)_{II}$, and strong $(C–C)_{III}$ stretches
947 (w)		Weak asynchronous $(C–H)_I$ and $(C–H)_{II}$ stretches with strong wagging, Weak $(C–C)_I$, weak $(C–C)_{II}$, and medium $(C–C)_{III}$ stretches
	985 (w)	Weak asynchronous $(C–H)_{II}$ stretches with medium $(C–H)_I$ and $(C–H)_{II}$ wagging, Weak $(C–C)_I$, strong $(C–C)_{II}$, and strong $(C–C)_{III}$ stretches
	1058 (m)	Medium asynchronous $(C–H)_I$ stretches With strong $(C–H)_I$ and medium $(C–H)_{II}$ wagging, Strong $(C–C)_I$ and weak $(C–C)_{II}$ stretches
	1216 (w)	Medium asynchronous $(C–H)_I$ and strong $(C–H)_{II}$ stretches with Medium $(C–H)_I$ and strong $(C–H)_{II}$ wagging, Medium $(C–C)_I$ and strong $(C–C)_{II}$ stretches
	1240 (w)	Weak asynchronous $(C–H)_I$ and strong $(C–H)_{II}$ stretches with Medium $(C–H)_I$ and strong $(C–H)_{II}$ wagging, Medium $(C–C)_I$, $(C–C)_{II}$, and $(C–C)_{III}$ stretches
	1260 (m)	Strong asynchronous $(C–H)_I$ and medium $(C–H)_{II}$ stretches With strong $(C–H)_I$ and medium $(C–H)_{II}$ wagging, Weak $(C–C)_I$ and medium $(C–C)_{II}$ and $(C–C)_{III}$ stretches
1286 (m)		Weak asynchronous $(C–H)_I$ and $(C–H)_{II}$ stretches With medium $(C–H)_I$ and weak $(C–H)_{II}$ wagging, Weak $(C–C)_I$, medium $(C–C)_{II}$, and weak $(C–C)_{III}$ stretches
	1355 (m)	Strong asynchronous $(C–H)_I$ and $(C–H)_{II}$ stretches With strong $(C–H)_I$ and medium $(C–H)_{II}$ wagging, Strong $(C–C)_I$, medium $(C–C)_{II}$, and weak $(C–C)_{III}$ stretches

TABLE III. *(Continued.)*

Theoretical IR	Theoretical Raman	Mode description
3012 (w, sh)	3012 (s)	Weak asynchronous $(C–H)_I$ and strong $(C–H)_{II}$ stretches with Weak $(C–H)_I$ and strong $(C–H)_{II}$ wagging, Weak $(C–C)_{II}$ and $(C–C)_{III}$ stretches
3025 (vs)	3025 (s)	Weak asynchronous $(C–H)_I$ and strong $(C–H)_{II}$ stretches with Weak $(C–H)_I$ and strong $(C–H)_{II}$ wagging, Weak $(C–C)_{II}$ and $(C–C)_{III}$ stretches
3094 (s)	3094 (s)	Strong asynchronous $(C–H)_I$ and medium $(C–H)_{II}$ stretches with Medium $(C–H)_I$ and weak $(C–H)_{II}$ wagging, Weak $(C–C)_I$ and $(C–C)_{III}$ stretches
3109 (s)	3109 (vs)	Strong asynchronous $(C–H)_I$ and medium $(C–H)_{II}$ stretches with Medium $(C–H)_I$ and weak $(C–H)_{II}$ wagging, Weak $(C–C)_I$ and $(C–C)_{III}$ stretches

from 3006 cm^{-1} to 3109 cm^{-1} associated with strong C–H stretches within the molecule. Note that the set of low frequency modes in the range from 560 cm^{-1} to 1355 cm^{-1} constitutes what is commonly known as the fingerprint region since it is unique for a particular hydrocarbon. The positions of these low frequency vibrational modes can easily be understood for octahedrane, as well as for other hydrocarbons, by realizing that the harmonic frequency of a particular vibrational mode is inversely proportional to the square root of the atomic mass of the relevant atom. Thus, modes involving basically carbon atoms are lower in frequency than those modes involving mainly hydrogen atoms since carbon is heavier than hydrogen.

A detailed listing of the calculated infrared and Raman frequencies along with a qualitative physical description of each vibrational mode is shown in Table III. While we have chosen to list and describe all of the theoretical infrared and Raman active modes that range in intensity from very strong to weak, there are a few modes which we wish to highlight in some detail. Octahedrane has a very characteristic Raman active breathing mode for the entire carbon core at 560 cm^{-1}, as well as two breathing modes along the central C_3 axis, which intersects the two cyclopropyl rings and the central equatorial cyclohexyl ring at 629 cm^{-1} (Raman active) and 926 cm^{-1} (infrared active).

We used both NRLMOL and NRL-TBMD to calculate the VDOS, and we have compared our results in Fig. 7. The agreement between the two VDOS plots when calculated using these two different approaches in the range between 400 cm^{-1} and 1400 cm^{-1} is actually quite good. At the higher frequencies, the C–H stretching modes differ between the two methods by about 7%. We have encountered this result before when using the NRLMOL and NRL-TBMD schemes to compute the VDOS for other test hydrocarbon cases, and we attribute it to the following observation. The

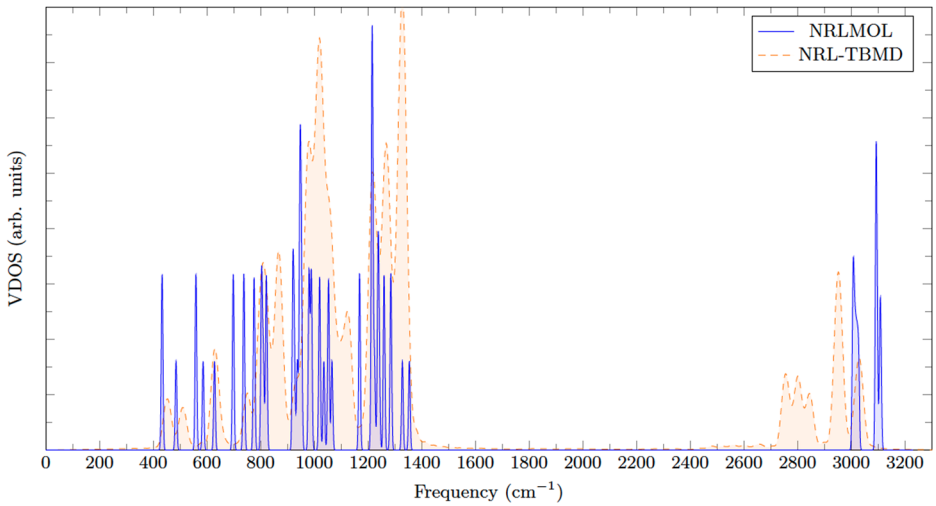

FIG. 7. Comparison of NRLMOL and NRL-TBMD vibrational densities of states (VDOS) for octahedrane. A temperature of 300 K was used for the MD simulation.

tight-binding parameters are fit to DFT results for a wide range of test systems containing carbon where the C–C bond lengths involve sp^2–sp^2 interactions (e.g., benzene), sp^3–sp^3 interactions (e.g., ethane), and sp-sp interactions (e.g., C_2), thus by construction the NRL-TBMD method is well-suited to handle the stretching of C–C bonds.

Regarding the C–H bonds, our tight-binding parameters were fit to data for C–H bond lengths between 0.5 and 2.0 Å. It is important to note that this fitting process emphasized the equilibrium bond distance and the low-frequency phonon modes, i.e., the curvature of the energy as a function of bond length near equilibrium, rather than the curvature at larger distances. Additional fitting could be done to improve the fit to high frequencies, but this might well impact the fit for lower frequency phonons.

In comparing our two methods to compute vibrational spectra, we see that the NRLMOL results are as accurate as any DFT method, while NRL-TBMD is also capable of handling long simulations of many atoms at finite temperature, specifically up to 648 atoms at 300 K for the 20 000 time steps used in this study. It is also very important to note that while both approaches give comparable results for optimized geometries, the NRL-TBMD approach is computationally cheaper and faster than NRLMOL. The NRL-TBMD scheme can also yield important mechanical and dynamical properties of solid octahedrane up to its melting temperature, and we are pursuing this study in an upcoming publication. As far as the vibrational properties of octahedrane are concerned, although both NRLMOL and NRL-TBMD yield VDOS spectra that are in reasonable agreement with each other, particularly in the fingerprint region, one still needs a DFT approach, like NRLMOL, to clearly discern which vibrational modes are infrared and Raman active and how they may be understood through a detailed physical mode analysis.

V. CONCLUSIONS

The vibrational properties of the novel caged polyhedral hydrocarbon, octahedrane, have been computed by two completely different theoretical methods: an all-electron Gaussian orbital DFT approach (NRLMOL) and a tight-binding scheme coupled with molecular dynamics (NRL-TBMD). Specifically, both schemes have yielded VDOS spectra which are in general good agreement with each other, especially in the fingerprint region of the spectra. The VDOS spectra computed by NRLMOL can be easily further decomposed to yield infrared and Raman spectra for octahedrane which can be compared with future experimental work.

The NRL-TBMD method has two key advantages over the NRLMOL approach: (i) NRL-TBMD is computationally faster and cheaper to implement than a full DFT scheme, like NRLMOL, and (ii) NRL-TBMD can easily be scaled up to perform larger scale calculations which are required for the detailed computational studies of the structural and dynamical properties of octahedrane in the crystalline phase at finite temperature. Since our calculated equilibrium geometries for the molecular octahedrane are in excellent agreement using both of these theoretical methods, we are particularly encouraged that the NRL-TBMD method will be capable of computing the mechanical and dynamical properties of solid octahedrane using less computational time and memory than conventional DFT approaches.

ACKNOWLEDGMENTS

D.F. acknowledges support from the Office of Naval Research-Naval Academy and Naval Research Laboratory Cooperative Program. M.J.M. is supported by the Kinnear Foundation and Duke University. S.L.R. is grateful for financial support from both the Office of Naval Research Summer Faculty Research Program and the STC Center for Integrated Quantum Materials, NSF Grant No. DMR-1231319, and he is particularly grateful to Noam Bernstein and Tunna Baruah for their assistance in resolving a number of technical issues encountered in compiling and running NRLMOL. S.L.R. also wishes to thank MIT and Professor Timothy M. Swager of MIT, in particular, for their financial assistance and hospitality as the 2016–2017 Dr. Martin Luther King, Jr. Visiting Professor of Chemistry at MIT. We thank Igor Mazin and C. Stephen Hellberg for their kind and professional assistance in the preparation of several of the figures in this paper.

REFERENCES

[1] C.-H. Lee, S. Liang, T. Haumann, R. Boese, and A. de Meijere, Angew. Chem., Int. Ed. Engl. **32**, 559 (1993).
[2] K.-i. Hirao, Y. Ohuchi, and O. Yonemitsu, J. Chem. Soc., Chem. Commun. **2**, 99 (1982).
[3] H. Okamoto, K. Satake, H. Ishida, and M. Kimura, J. Am. Chem. Soc. **128**, 16508 (2006).
[4] A. de Meijere, C.-H. Lee, M. A. Kuznetsov, D. V. Gusev, S. I. Kozhushkov, A. A. Fokin, and P. R. Schreiner, Chem.–Eur. J. **11**, 6175 (2005).
[5] P. Hohenberg and W. Kohn, Phys. Rev. **136**, B864 (1964).
[6] W. Kohn and L. Sham, Phys. Rev. **140**, A1133 (1965).
[7] R. J. Ternansky, D. W. Balogh, and L. A. Paquette, J. Am. Chem. Soc. **104**, 4503 (1982).
[8] A. Karton, P. R. Schreiner, and J. M. Martin, J. Comput. Chem. **37**, 49 (2016).
[9] D. Finkenstadt, G. Pennington, and M. J. Mehl, Phys. Rev. B **76**, 121405 (2007).
[10] D. Finkenstadt, G. Pennington, and M. J. Mehl, MRS Proc. **1057**, 10 (2007).
[11] S. L. Richardson and J. L. Martins, Phys. Rev. B **58**, 15307 (1998).
[12] J. Kortus, M. R. Pederson, and S. L. Richardson, Chem. Phys. Lett. **322**, 224 (2000).
[13] S. L. Richardson, T. Baruah, M. J. Mehl, and M. R. Pederson, Chem. Phys. Lett. **403**, 83 (2005).
[14] S. L. Richardson, T. Baruah, M. J. Mehl, and M. R. Pederson, Diamond Relat. Mater. **15**, 707 (2006).
[15] J. P. Perdew, K. Burke, and M. Ernzerhof, Phys. Rev. Lett. **77**, 3865 (1996).
[16] J. P. Perdew, K. Burke, and M. Ernzerhof, Phys. Rev. Lett. **78**, 1396 (1997).
[17] G. A. Shamov, P. H. Budzelaar, and G. Schreckenbach, J. Chem. Theory Comput. **6**, 477 (2010).
[18] P. R. Schreiner, A. A. Fokin, R. A. Pascal, and A. de Meijere, Org. Lett. **8**, 3635 (2006).
[19] M. R. Pederson and K. A. Jackson, Phys. Rev. B **41**, 7453 (1990).
[20] K. A. Jackson and M. R. Pederson, Phys. Rev. B **42**, 3276 (1990).
[21] M. R. Pederson and K. A. Jackson, Phys. Rev. B **43**, 7312 (1991).
[22] R. E. Cohen, M. J. Mehl, and D. A. Papaconstantopoulos, Phys. Rev. B **50**, 14694 (1994).
[23] M. J. Mehl and D. A. Papaconstantopoulos, Phys. Rev. B **54**, 4519 (1996).
[24] M. J. Mehl and D. A. Papaconstantopoulos, in *Topics in Computational Materials Science*, 1st ed., edited by C. Fong (World Scientific, Singapore, 1998), Vol. 1, Chap. 5, pp. 169–213.
[25] D. A. Papaconstantopoulos and M. J. Mehl, J. Phys.: Condens. Matter **15**, R413 (2003), and references therein.

[26]M. J. Mehl and D. A. Papaconstantopoulos, in *Handbook of Materials Modeling*, 1st ed., edited by S. Yip (Springer, The Netherlands, 2005), Vol. 1, p. 275.
[27]D. A. Papaconstantopoulos and M. J. Mehl, in *Encyclopedia of Condensed Matter Physics*, edited by G. Bassani (Elsevier, Oxford, UK, 2005), Vol. 6, p. 194.
[28]M. R. Pederson, D. V. Porezag, J. Kortus, and D. C. Patton, Phys. Status Solidi B **217**, 197 (2000).
[29]A. Shabaev, S. G. Lambrakos, N. Bernstein, V. L. Jacobs, and D. Finkenstadt, "Initial construction of a general framework for numerical simulation of IED detection and remote activation scenarios," DTIC Document, NRL Memorandum Report NRL/MR/6390–10-9260, 2010.
[30]A. Shabaev, S. G. Lambrakos, N. Bernstein, V. L. Jacobs, and D. Finkenstadt, Appl. Spectrosc. **65**, 409 (2011).
[31]A. Shabaev, S. G. Lambrakos, N. Bernstein, V. L. Jacobs, and D. Finkenstadt, J. Mater. Eng. Perform. **20**, 1536 (2011).
[32]A. Shabaev, S. G. Lambrakos, N. Bernstein, V. L. Jacobs, and D. Finkenstadt, Proc. SPIE **8023**, 80230W-1–80230W-8 (2011).
[33]D. Finkenstadt, S. G. Lambrakos, N. Bernstein, V. L. Jacobs, L. Huang, L. Massa, and A. Shabaev, Int. J. Intell. Def. Support Syst. **5**, 24 (2012).
[34]R. P. Feynman, Phys. Rev. **56**, 340 (1939).
[35]P. Pulay, Mol. Phys. **17**, 197 (1969).
[36]D. Porezag and M. R. Pederson, Phys. Rev. B **54**, 7830 (1996).
[37]M. Pederson, A. Quong, J. Broughton, and J. Feldman, Comput. Mater. Sci. **2**, 536 (1994).
[38]A. Briley, M. R. Pederson, K. A. Jackson, D. C. Patton, and D. V. Porezag, Phys. Rev. B **58**, 1786 (1998).
[39]F. Kirchhoff, M. J. Mehl, N. I. Papanicolaou, D. A. Papaconstantopoulos, and F. S. Khan, Phys. Rev. B **63**, 195101 (2001).
[40]See http://cst-www.nrl.navy.mil/bind/dodtb/ for the DoD-parallel tight-binding molecular-dynamics code.
[41]D. Finkenstadt, N. Bernstein, J. L. Feldman, M. J. Mehl, and D. A. Papaconstantopoulos, Phys. Rev. B **74**, 184118 (2006).
[42]D. A. Papaconstantopoulos, M. J. Mehl, S. C. Erwin, and M. R. Pederson, in *Tight-Binding Approach to Computational Materials Science*, edited by P. Turchi, A. Gonis, and L. Colombo (MRS, Pittsburgh, 1998), Vol. 491, p. 221.
[43]O. K. Andersen, Phys. Rev. B **12**, 3060 (1975).
[44]D. J. Singh, H. Krakauer, and C. S. Wang, Phys. Rev. B **34**, 8391 (1986).
[45]J. M. Dickey and A. Paskin, Phys. Rev. **188**, 1407 (1969).
[46]J. Echeverria, G. Aullon, D. Danovich, S. Shaik, and S. Alvarez, Nat. Chem. **3**, 323 (2011).
[47]P. Rotkiewicz, iMol Molecular Visualization Program, http://www.pirx.com/iMol, 2007.